Chapter 2

Quantum and electrochemical interplay in hydrogenated graphene

The design of electrochemically gated graphene field-effect transistors for detecting charged species in real time, greatly depends on our ability to understand and maintain a low level of electrochemical current. Here, the interplay between the electrical in-plane transport and the electrochemical activity of graphene is explored. The addition of one H-sp^3 defect per hundred thousand carbon atoms reduces the electron transfer rate of the graphene basal plane by more than five times while preserving its excellent carrier mobility. Remarkably, the quantum capacitance provides insight into the changes of the electronic structure of graphene upon hydrogenation, which predicts well the suppression of the electrochemical activity based on the non-adiabatic theory of electron transfer. Thus, our work unravels the interplay between the quantum transport and electrochemical kinetics of graphene and suggests hydrogenated graphene as a potent material for sensing applications with performances going beyond previously reported graphene transistor-based sensors.

This chapter was published as an article: Lin Jiang, Wangyang Fu, Yuvraj Y. Birdja, Marc T. M. Koper, Grégory F. Schneider, *Nat. Commun.* **2018**, 9, 793.

2.1 Introduction

Graphene is unique among other solid-state materials in that all carbon atoms are located on the surface, making the graphene surface highly sensitive for the detection of changes in the environment. Particularly, the concept of electrochemically gated graphene field-effect transistor (GFET) enables the label-free detection of charged molecules on a small footprint upon their bindings at/near the graphene surface:[1] a binding event modulates the electrical current in the graphene channel through the local variation of the electric field[2]. The creation of practical electrochemically gated GFETs for detecting charged species, however, greatly depends on our ability to understand and maintain a low level of electrochemical current. Specifically, the electrochemical current rests on the current flowing between the graphene channel and redox active molecules in the solution phase.

Complementary to the GFET sensors, the electrochemical current towards a redox probe in solution has been widely studied and is at the basis of graphene electrochemical (GEC) sensors. Previous studies have revealed that the electrochemical activity is largely sensitive to the intrinsic chemical structure of the graphene basal plane.[3] Among the multiple approaches used to chemically modify graphene, for example, post-growth chemical modifications using various oxidative reactions[4] are effective routes to incorporate oxygen atoms, although at the cost of a poor control over the chemical structure of the resulting functional groups (i.e., epoxy, carbonyl, carboxylic acid, alcohol, all at the same time). Particularly, hydrogenated or fluorinated graphene endows a large range of possibilities to progressively tweak graphene with sp^3 defects without significantly pinning the lattice integrity or breaking the resilient basal plane C-C bonds.[5]

Here, a low density of H-sp^3 defects are introduced into monolayer graphene using a hydrogen plasma. Only one second of plasma treatment is able to render a pristine graphene surface (with few H-sp^3 defects) from the as-grown graphene (referred as untreated graphene) by removing the adsorbed hydrocarbons at the surface, as manifested by the dramatic boost in the electron transfer rate. Importantly, further addition of only one H-sp^3 defect per hundred thousand carbon atoms (more than 1 s of hydrogen plasma), allows us to substantially reduce the electron transfer rate of hydrogenated graphene (H-graphene) compared to untreated graphene. Remarkably, the degradation of the electrochemical kinetics of the graphene basal plane was successfully correlated with the density of states (DOS) by tuning the density of H-sp^3 defects. Although the H-sp^3 termination could contribute to a higher electrochemical activity, the electronic structure (DOS) in graphene plays an even more decisive role

in the rate of electron transfer between graphene and redox probes for a low defect density, indicating a non-adiabatic transfer process on the graphene basal plane.

2.2 Results

2.2.1 Raman characterization

To determine the density and the nature of the defects induced by hydrogen radicals, Raman spectroscopy (Figure 2.1a) and mapping (Figure AI. 1a) characterization was conducted on graphene prepared by chemical vapor deposition (CVD). The similarities between the Raman spectra for both CVD and exfoliated graphene (Figure AI. 2) indicate that the defects induced by the H_2 plasma – particularly the defect density n_D – are respectively equivalent. Importantly, the D peak at ~1340 cm^{-1}, due to single phonon intervalley scattering events, is caused by the apparition of H-sp^3 defects.[6] After a hydrogenation time of 10 s, a D' peak at 1620 cm^{-1} appears in the Raman spectrum as a shoulder of the G peak. The D' peak also associates with H-sp^3 defects.[7] The values determined for $I(D)/I(D')$ (~10) after 30 s and 60 s of hydrogenation are consistent with previous report and confirm the sp^3 nature of hydrogenated defects (Figure 2.1b).[8] Meanwhile, the intensity ratio $I(2D)/I(G)$, a sensitive parameter to graphene doping, decreases continuously from 2.2 to 1.3 upon extended hydrogenation (see Figure 2.1b).[9]

Derived from the $I(D)/I(G)$ ratio (a quantitative indicator of point defects in graphene samples),[10] the defect density n_D increases linearly with hydrogenation time from $n_D = (0.2 \pm 0.3) \times 10^{10}$ cm^{-2} at 0 s (untreated graphene) to $n_D = (3.2 \pm 0.7) \times 10^{11}$ cm^{-2} at 60 s, corresponding to a decrease in average distance between defects sites (L_D) from 122.6 nm to 10.0 nm (Figure 2.1c, see Appendix I. 2 for the calculation of n_D and L_D). Notably, the Raman mapping (D peak intensity) in Figure AI. 1b on exfoliated graphene flakes (which contains minimal native defects, except for edges), confirms the uniform defect distribution upon hydrogenation. Other surface characterizations including scanning electron microscopy (SEM) and atomic force microscopy (AFM) (Figure AI. 3) further revealed the non-cracked and preserved lattice of H-graphene. Moreover, the low defect densities are also in agreement with the relatively small variations observed for the full width at half maximum (FWHM) of the D and G peaks (2-5 cm^{-1}, Figure 2.1e).[22] In addition, the peak broadening as hydrogenation proceeds is mainly due to the shortened lifetime of phonons caused by increasing amounts of defects.[10-11]

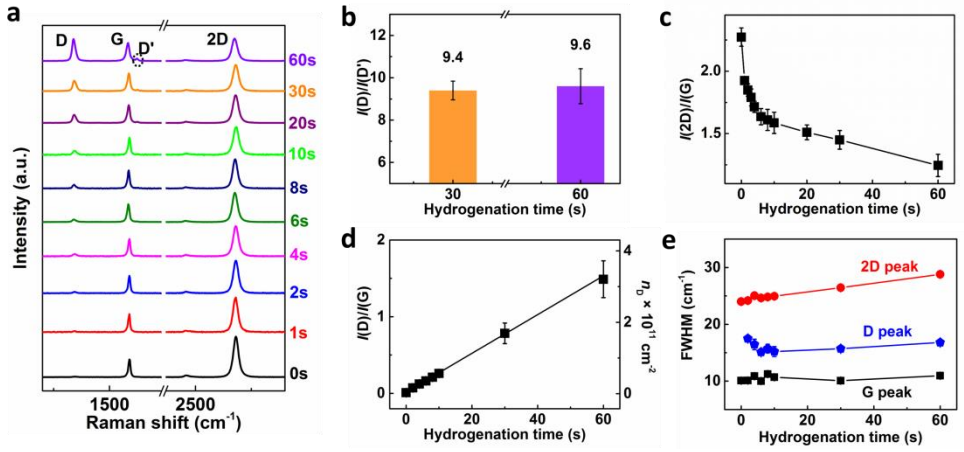

Figure 2.1 Raman characterization of hydrogenated graphene. a) Averaged Raman spectra of CVD graphene on a Si/SiO_2 substrate after 0-60 s of H_2 plasma (10 W, 1.0 mbar). b) The intensity ratio $I(D)/I(D')$ after 30 s and 60 s of hydrogenation. c) The intensity ratio $I(2D)/I(G)$ for hydrogenation times ranging from 0 to 60 s. d) The intensity ratio $I(D)/I(G)$ and the derived defect density n_D, plotted vs the hydrogenation time. The error bars include results from both exfoliated and CVD graphene. e) The FWHM of the 2D, G, and D peaks vs the hydrogenation time. The spectra are recorded using a 2.33 eV (532 nm) laser excitation. The error bars in (b–e) are the standard deviation of experimental values.

2.2.2 Electron transport measurement

High-quality, large-area CVD graphene was used for the device fabrication following a facile and clean fabrication strategy as illustrated in Figure 2.2a (see also Methods for details).[12] Specifically, the topside of CVD graphene (at Cu foil) was first glued on the supporting glass substrate and protected by the photopolymer of pentaerythritol tetra(3-mercaptopropionate) and triallyl-1,3,5-triazine-2,4,6-trione (PETMP–TATATO).[13] After the removal of backside graphene (by oxygen plasma), the copper ends were protected by covering them with a film of cellulose acetate butyrate (CAB). Then the graphene surface was exposed by etching the Cu in a solution of ammonium persulfate, followed by a series of hydrogen plasma treatments to introduce defects with controlled densities. During the procedure, a low-temperature annealing process (110°C for ~1-3 h) was employed to ensure a good adhesion of graphene on the underlying polymer substrate. Only the fabricated graphene devices exhibiting mobilities on the order of 1000 – 1500 $cm^2 V^{-1} s^{-1}$ went through a series of field-effect, quantum capacitance, and cyclic voltammetry (CV) experiments immediately after each hydrogenation treatment. To rule out any possible sample-to-sample variations, all the aforementioned measurements were conducted on the same graphene samples.

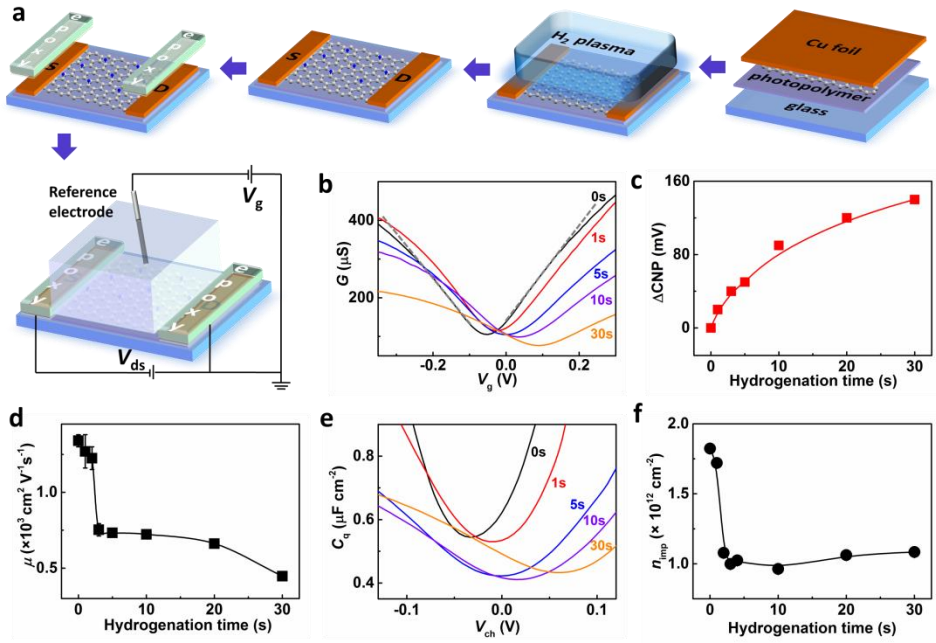

Figure 2.2 Transport characteristic and quantum capacitance of CVD graphene upon hydrogenation. a) Illustration of the field effect transistor setup fabricated from CVD graphene. b) Room temperature conductance (G) plots as a function of the gate voltage (V_g) showing the p-doping effect upon hydrogenation from 0 to 30 s. The gray dashed line is a guide-to-the-eye, highlighting the sublinear behavior of the $G(V_g)$ curves. c) The shifts of the charge neutrality point (CNP) upon hydrogenation. d) The carrier mobility of graphene, μ, vs the hydrogenation time. e) Quantum capacitance C_q of graphene measured as a function of V_{ch} for 0–30 s of hydrogenation. f) Impurity density n_{imp} vs hydrogenation time. The electrolyte solution is 0.1 M KCl with 10 mM Tris (pH 8). The error bars in (d, f) are the standard deviation of experimental values.

Figure 2.2a depicts a GFET device with a source (S) and a drain (D) electrode bridged via a conductive graphene channel. A gate voltage (V_g) is applied to the electrolyte solution via a Ag/AgCl reference electrode, to modulate the conductivity (G) of the GFET. Specifically, when the V_g is swept from negative to positive, the Fermi level (E_F) of graphene shifts from the valence band (hole carriers) to the conduction band (electron carriers). At the so-called charge neutrality point (CNP), the concentration of hole carriers equals that of electron carriers and the conductivity of graphene reaches its minimum G_{min} (Figure 2.2b). The slopes of the sublinear $G(V_g)$ curves are the measure for the carrier mobility μ, while the observed negative voltage of the CNP for

untreated graphene implies an electron (n) doping induced by the underlying photopolymer substrate.

As hydrogenation proceeds, the CNP continuously shifts to more positive voltages, a characteristics of hole (p) doping. This doping effect can be attributed to water adsorption, which occurs more readily on H-graphene than on untreated graphene.[5b, 14] Upon 1 s hydrogenation, graphene exhibits a slightly increased $G_{\min}$ (Figure 2.2b) and a rather stable carrier mobility μ (Figure 2.2d), suggesting that the mild hydrogenation treatment barely influence – even improves – the electrical properties of graphene.[36] As a result, the H radicals after only one second of hydrogenation are hypothesized to yield a cleaner graphene by effectively removing hydrocarbon adsorbates on the surface.[37] Further hydrogenation reduces the mobility μ (and $G_{\min}$) of graphene down to $\sim$750 cm^2 V^{-1} s^{-1} (after 2 to 5 s of hydrogenation), after which μ stabilizes at 450-660 cm^2 V^{-1} s^{-1} (after 5 to 30 s of hydrogenation). As a result, the carrier mobility in graphene is mostly sensitive to the introduction of one H-sp^3 scattering centre per $\sim$250,000 down to $\sim$145,000 sp^2 hybridized carbon atoms (correspondingly $L_{\mathrm{D}} = 45$ down to 35 nm). In addition to the sublinear behavior of the $G(V_{\mathrm{g}})$ curves (even after a series of hydrogenation), the remarkable decrease of $G_{\min}$ also suggests that the conductivity of (hydrogenated) graphene is dominated by the short-range scattering mechanism.[15] Such an observation is also confirmed by previous work in which hydrogenation introduced short-range scatterings in graphene lattice.[16]

2.2.3 Quantum capacitance measurement

As a direct manifestation of the Pauli exclusion principle, the quantum capacitance effect in graphene is particularly prominent due to its low density of states (DOS).[17] The quantum capacitance C_{q} of graphene, can be directly determined as a function of the channel potential across the graphene sheet V_{ch} using an electrochemical configuration (see Figure AI. 4).[18] In Figure 2.2e, the measured C_{q} generally displays a broad minimum, $C_{\mathrm{q,min}}$, at the voltage of CNP and linearly increases with V_{ch} on both sides of the CNP. Similar to the conductivity changes after hydrogenation (Figure 2.2b), the V-shaped $C_{\mathrm{q}}(V_{\mathrm{ch}})$ curves exhibit not only positive CNP shifts, but also broader and decreased minimums, as well as more creeping increases of C_{q} with the voltage. In nature $C_{\mathrm{q,min}}$ is directly related to the density of effective charged impurities, n^* (since these impurities can cause local potential fluctuations in graphene), which can reveal the global behavior of defects in graphene (see Appendix I. 3).[9a] Notably, our reported capacitance values are generally lower than those reported in previous studies. The difference is ascribed to the cleanness of our

graphene surface, which gives a $n^* = 9.73 \times 10^{10}$ cm^{-2}, ~8 time lower than, for example, CVD graphene on SiO_2/Si wafer ($n^* = 8.0 \times 10^{11}$ cm^{-2}).[18] Such a remarkably lowered n^* can be ascribed to our clean fabrication strategy (see Methods) which introduces less charged impurities, or reflects the differences between the substrates, which could lead to different degrees of charge transfer.

More importantly, the effective charged concentration n^* can be related to the impurity density n_{imp}, referred as the impurities at the interfaces between graphene and the substrate, or between graphene and air, or resulting from the intrinsic defects caused by the growth or transfer process of CVD graphene (see Appendix I. 3 for details). In Figure 2.2f, n_{imp} decreases in the first 5 s and then settles till 30 s hydrogenation, a scenario suggesting that the mild hydrogenation (within 1-5 s) sweeps away the trapped/adsorbed charge impurities at graphene interfaces. The evolution of the defect density n_D and of the impurity density n_{imp} are closely related and critical to the electron transport and electrochemical kinetics, which will be discussed in more detail below (see Correlation of n_{D} with n_{imp}).

2.2.4 Electrochemical kinetics measurement

Cyclic voltammetry (CV) was employed to investigate the electrochemical behavior of H-graphene. Specifically, the hexaammineruthenium (II)/hexaammineruthenium (III) redox couple, $Ru(NH_3)_6^{2+/3+}$, was adopted as an outer-sphere redox mediator: i) it is surface insensitive and thus the electron transfer from the mediator to graphene (vice versa) mainly relies on the electronic structures of electrode and the mediator itself, and ii) it possesses a standard potential in the vicinity of the Fermi level of graphene.[19]

From the CVs in Figure 2.3a, the electrochemical activity of graphene towards the redox probe before and after 1-30 s of hydrogenation was determined. The current densities (j) of the oxidation peak (at –170 mV) and reduction peak (at –290 mV) show that 1 s of hydrogenation is sufficient to increase the electrochemical activity of graphene by a factor of 4 compared to untreated graphene, while further hydrogenation brings about an immediate decrease of activity. The peak-to-peak separation (ΔE_{p}), a qualitative indicator of the electrochemical reversibility in graphene, displays a minimum at 1 s hydrogenation time in accordance with the current density (Figure AI. 5c).

Furthermore, from the data in Figure 2.3b the heterogeneous electron transfer rate (k^{o}) between the graphene basal plane and the redox probe was extracted to quantitatively evaluate the electrochemical kinetics of graphene upon hydrogenation.

Specifically, ΔE_p of the quasi-reversible redox peaks are below 220 mV as the scan rate (v) increases, which meets the criteria of the Nicholson's method to estimate the kinetic parameters[19-20] (See Appendix I. 4). Consistent with the current density depicted in Figure 2.3a, the deduced values of k^o exhibit a peaked behavior as a function of the hydrogenation time (Figure 2.3c). In details, k^o increases by up to ~12 fold (6.77×10^{-4} cm s^{-1}) after one second of hydrogenation compared to untreated graphene (5.37×10^{-4} cm s^{-1}). For longer hydrogenation times, k^o sharply drops down to $\sim 1.70 \times 10^{-4}$ cm s^{-1} within 5 s and stabilizes at 1.50×10^{-4} cm s^{-1} after 30 s hydrogenation. Such a trend is reproducible for different batches (see Figure AI. 5a-b and Appendix I. 5).

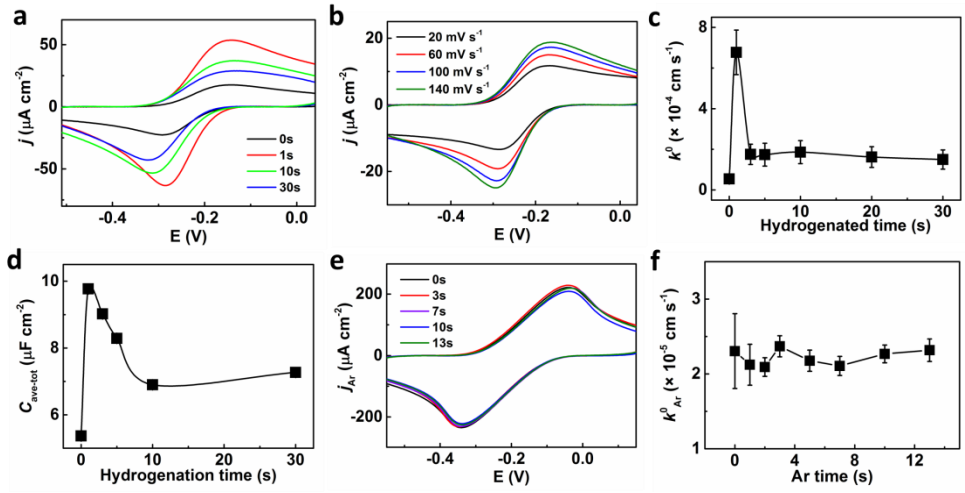

Figure 2.3 Electrochemical behavior of CVD graphene upon hydrogenation. a) Cyclic voltammograms (CVs) obtained on graphene after 0–30 s of hydrogenation at a scan rate of 100 mV s^{-1}. b) Current density vs scan rate for untreated graphene shown in a. c) The electron transfer rate k^o vs hydrogenation time from 0 to 30 s. d) The averaged total capacitance $C_{ave-tot}$ vs hydrogenation time from 0 to 30 s. e) CV curves obtained on graphene after 0–13 s of Ar treatment at a scan rate of 100 mV s^{-1}. f) k^o_{Ar} vs argon plasma treating time from 0 to 13 s. The aqueous electrolyte solution contains 0.1 M KCl supplemented with 10 mM Tris at pH 8. The redox probe employed is 1 mM hexaammineruthenium (II)/hexaammineruthenium (III) chloride. The error bars in (c, d, f) are the standard deviation of experimental values.

The total electrical capacitance (C_{tot}) per unit area of graphene, consists of the electrical double layer capacitance (C_{dl}) and the graphene quantum capacitance (C_q) connected in series[21]. C_{tot} can be obtained either by using a lock-in technique (see Methods) or by measuring the capacitive CV current for different scan rates, which is an averaged evaluation over a relatively wide potential ($C_{ave-tot}$, Figure AI. 6 and Appendix I. 6). Additionally, the basic rectangular shapes of the capacitive current curves imply purely capacitive behavior without Faradaic processes. Furthermore,

upon hydrogenation $C_{\mathrm{ave-tot}}$ first increases after 1 s, then drops till 10 s and saturate till 30 s, varying similarly as k^{o} (Figure 2.3d). The observed changes in $C_{\mathrm{ave-tot}}$ can be mainly attributed to the DOS variations with hydrogenation (as C_{q} dominates in the series circuit).

2.2.5 Electrochemistry of H-sp³ vs vacancy defects

To further evaluate the exact impact of defects on the electrochemical kinetics of graphene, samples that were treated with an argon plasma (referred as Ar-graphene) was studied with comparable defect densities as to hydrogenated graphene (Figure AI. 7 and Appendix I. 7). In contrast to the sensitive electrochemical behavior in H-graphene (Figure 2.3a, c), both the current density and k^{o} on Ar-graphene show negligible sensitivity to the argon plasma treatment (Figure 2.3e, f). Such trends are consistent with the previous report that a low density of vacancy defects hardly impacts the electrochemical activity of graphene[22].

Based on the different $I(\mathrm{D})/I(\mathrm{D}')$ ratios characterized using Raman spectroscopy (i.e., ~7 for Ar-graphene and ~10 for H-graphene),[23] argon plasma is identified to forms vacancy defects by removing carbon atoms, while hydrogenation changes graphene hybridization from sp^2 to sp^3. Thus, the insight is gained into the driving mechanism for the observed electrochemical behavior. Rather than the vacancy defect, the change of hybridization (in H-graphene) is closely related to the electrochemical properties of hydrogenated graphene (Figure 2.3). Meanwhile, coincident to the boost of k^{o}, the G_{min} and μ increase slightly after 1 s of hydrogenation (Figure 2.2), indicating a cleaner graphene with less surface scattering centers: hydrogen radicals are expected to react with the hydrocarbons adsorbed on the surface of graphene. Such a cleaning effect is due to the much higher reactivity of hydrocarbons with hydrogen radicals compared to the reactivity of the graphene itself with the same radicals. As airborne contaminations, hydrocarbons can adsorb onto any surface, as revealed from the observation that the wetting of graphitic surface dramatically changes over short time periods[24]. Indeed, such cleaning effect is in agreement with prior observations that graphite – more specifically freshly exfoliated highly oriented pyrolytic graphite – exhibits high but instantly decaying electrochemical activity due to the exposure to airborne contaminants.[25] Notably, no cleaning effect using argon plasma under our condition is expected (ion energy ~60 eV)[26], as also confirmed by the high-resolution transmission electron microscopy images of Ar-graphene (not shown here).

In addition, X-ray photoelectron spectroscopy (XPS, Figure AI. 8 and Appendix I. 8) in complementary to Raman was employed to compare graphene containing similar

defect densities (according to Raman analysis) after 60 s of hydrogenation and after 15 s of argon plasma treatment. The presence of C-sp^2 (284 eV), C-sp^3 (285 eV), C–O (286 – 286.2 eV), and C = O (287.8 – 288 eV) in C 1*s* spectra, suggest that both samples contain sp^2 and sp^3 carbon with minor oxygen contaminants from PMMA residues (only used for XPS samples to transfer graphene onto the Si substrate). As XPS probes both the surface chemistry of graphene and its surface adsorbents, a higher content of sp^3 carbon was observed from XPS analysis (Table AI. 1), compared to the results of Raman spectroscopy. Thus, the observed sp^3 C in both H-graphene (6.2–8.0%) and Ar-graphene (3%) is ascribed to possible surface adsorbents including PMMA residues and hydrocarbons. A trace amount of sp^3 doping in the graphene lattice (up to 0.8% sp^3 C in H-graphene) was, however, determined by Raman spectroscopy.

2.2.6 Correlation of n_D with n_{imp}

To shed light on the influence of the electrochemical current on the performance of GFET sensors, the interplay between the in-plane charge transport and the electrochemical activity of H-graphene is discussed here. Particularly, the correlations between the DOS, the mobility of charge carriers μ, and the electron transfer rate k^o, with respect to the density of charged impurity n_{imp} and defect density n_{D} are systematically investigated. Finally, a comprehensive discussion on the driving mechanism for the electrical and electrochemical behavior observed for H-graphene is provided.

To understand the correlation between defect density n_{D} and impurity density n_{imp} (presented in Figure 2.4a), it is important to consider their relation to the electronic properties of graphene. It is well-known from studies on supported graphene that defects yield short-range electron scattering in graphene. Impurities, on the other hand, cause long-range (Coulomb) scattering resulting in trapped electron states. The overall conductivity of graphene is dictated by the prevalence of either impurities or defects in the sample; n_{D} dominates at high charge carrier density while n_{imp} leads at low density regime.[15b, 27] Impurities are generally present on the graphene-air surface or at the interface between graphene and the underlying substrate. The cleaning effect in the first second of hydrogenation appears in Figure 2.4a as the decreasing onset for n_{imp} (from 9.05 to 8.52×10^{12} cm^{-2}).

Aside from the cleaning effect, the subsequent drop in n_{imp} from 8.52×10^{12} cm^{-2} to 5.01×10^{12} cm^{-2} occurs as hydrogenation induces changes in hybridization from sp^2 to sp^3, steadily increasing n_{D}. The presence of sp^3 hybridized spots in the lattice causes the lattice to expand and to curve. The increased distance between the lattice

and substrate-related impurities explains the sharp drop in n_{imp}. Further on, n_{imp} slightly increases (from 5.01×10^{12} cm^{-2} to 5.31×10^{12} cm^{-2}), which can be ascribed to the accumulation of trapped water molecules at the graphene surface, accompanying the increasing n_{D} ($n_{\mathrm{D}} > (2.6 \pm 0.5) \times 10^{10}$ cm^{-2}).

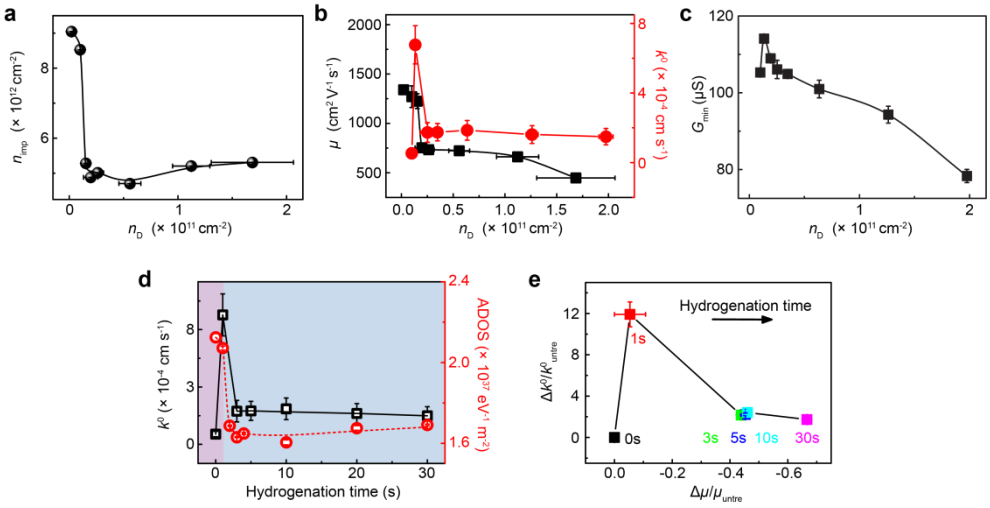

Figure 2.4 Quantum and electrochemical interplays in hydrogenated graphene. a) The dependence of n_{imp} on n_{D}. b) Correlations of μ and k^{o} with n_{D}, respectively. c) The minimum conductivity (G_{min}) vs n_{D}. d) The correspondence between ADOS and k^{o} as a function of the hydrogenation time. The purple region represents the cleaning-dominated regime and the blue region represents the regime where the chemical modification dominates. e) The relative variations of $\Delta\mu/\mu_{\mathrm{untre}}$ correlating with $\Delta k^{\mathrm{o}}/k^{\mathrm{o}}_{\mathrm{untre}}$ according to the corresponding hydrogenation time. The subscript "untre" represents the untreated graphene. The error bars are the standard deviation of experimental values.

2.2.7 Correlation of k^o and μ with n_D

The first report on the correlation of k^{o} with the density of vacancy defects in monolayer graphene showed that k^{o} remained constant at low densities but underwent a tenfold increase at a defect density of 10^{12} cm^{-2} ($I_{\mathrm{D}}/I_{\mathrm{G}} \cong 2.95$).[22] However, the high density of vacancy defects lowers the electrical performance of graphene. In our work, k^{o} is improved up to 12-fold (to 6.77×10^{-4} cm s^{-1}) at a low H-sp^3 defect density of $n_{\mathrm{D}} = (1.0 \pm 0.1) \times 10^{10}$ cm^{-2} ($I_{\mathrm{D}}/I_{\mathrm{G}} \cong 0.4$). Then, when n_D continues to rise, k^{o} drops sharply to stabilize between $1.5 - 1.7 \times 10^{-4}$ cm s^{-1} (red line, Figure 2.4b).

Separately, when k^{o} increases, the carrier mobility μ stays unchanged (or becomes slightly higher) compared to untreated graphene (black line, Figure 2.4b) at $n_{\mathrm{D}} =$

$(1.0 \pm 0.1) \times 10^{10}$ cm^{-2}. With the continuous growth of defect density up to $n_{\mathrm{D}} = (2.0 \pm 0.7) \times 10^{10}$ cm^{-2}, μ exhibits a deep drop, indicating that the carrier transport in graphene is sensitive to the existence of even low densities of H-sp^3 defects ($n_{\mathrm{D}} \leq 2.0 \times 10^{10}$ cm^{-2} corresponds to inter-distance L_{D} of ~40 nm). For higher defect densities, however, the decrease of μ is less pronounced (till $n_{\mathrm{D}} = (1.7 \pm 0.4) \times 10^{11}$ cm^{-2}, that is L_{D}~14 nm). The minimum conductivity (G_{min}) changes with n_D in Figure 2.4c, correlating well with the fluctuations in mobility (Figure 2.4b).

Based on Boltzmann theory, the conductivity of graphene (G) is proportional to $1/\sqrt{n_{\mathrm{D}}}$ at high carrier density (far from the CNP).[28] In consequence, μ is expected to decrease with increasing n_{D} upon hydrogenation, while at low carrier density (near the CNP), G is proportional to $\sqrt{n_{\mathrm{imp}}}$ and G_{min} is expected to reduce with the decrease of n_{imp}. The data in Figure 2.4b,c follow to the theory, except for the increase in both G_{min} and μ at the initial dose of hydrogenation ($n_{\mathrm{D}} = (1.0 \pm 0.1) \times 10^{10}$ cm^{-2}). This can be explained by considering the cleaning of adsorbates from the graphene surface. To be specific, hydrogenation introduces H-sp^3 defects while also removing surface short-range scatterers outweighing the effect on the conductivity and mobility of graphene. Separately, the decrease of ADOS after hydrogenation contributes to the decrease of intrinsic charge carrier density *n* rather than affecting the carrier mobility in graphene.

2.2.8 Correlation between the DOS and k^o

In electrochemistry, the kinetics of electron transfer from graphene to a redox probe is dependent on the electrochemical potential of electrons in graphene (that is the Fermi level, E_{F}) with respect to the electrochemical potential of the redox couple in solution.[17, 29] For example, for the electron to flow from the graphene to the redox probe, the graphene E_{F} that can be tuned by varying the potential applied to the graphene electrode or by sweeping the gate voltage, should at least align with the LUMO level of the oxidative molecule to allow an efficient electron transfer. For a non-adiabatic process, the DOS in graphene decides – whether or not – a basal plane electron could tunnel to the redox probe. Practically, the electron transfer occurs when the electronic resonance between the redox molecule and graphene is reached, that is for a given value of the applied potential, and is measured by studying how fast the electron transfer reaction can reach its equilibrium (*kinetics*).[30] In short, the electrochemical kinetics (reflected by k^{o}) of graphene relies on the DOS on the premise of non-adiabatic electron transfer.

In 2D materials like graphene, its minimal quantum capacitance, $C_{\mathrm{q,min}}$, can be used to deduce its average DOS (ADOS) at a specific E_F: $\langle\rho\rangle = C_{\mathrm{q,min}}/e^2$, where e is the

electron charge.[31] The change of ADOS with k^o as hydrogenation proceeds is plotted and compared in Figure 2.4d. During the first second (within the grey region), the ADOS decreases a little, however k^o increases dramatically, which can be mainly ascribed to the volatilization of hydrocarbon contaminants. That is, the hydrogen radicals first remove the hydrocarbon adsorbates to reveal the electrochemical activity of the underlying graphene, as the kinetic process involves interface-sensitive electron tunneling. Notably, H radicals can also attack the graphene lattice during the hydrocarbon cleaning and the resulted H-sp^3 defects could lead to the observed decrease in the ADOS.[22] Upon further hydrogenation (the beginning of the green region), the ADOS and k^o decrease sharply, which are mainly due to the modification of graphene basal plane by hydrogen radicals. The decay of k^o with DOS is in concordance with the non-adiabatic electron transfer, in which the rate depends on the electronic properties of the electrode due to the weak electronic interaction between the redox mediator and the electrode, according to the Levich–Dogonadze theory[32] and Fermi's golden rule[33]. It is of note here that the decrease in k^o (Figure 2.4d) is unlikely due to H-sp^3 termination, as the formed C-H dipole is more susceptible towards nucleophilic attack,[34] which could increase the electrochemical activity. Nor is it likely that the kinetics were affected by surface oxidation during exposure to air: XPS spectra on hydrogenated graphene demonstrate stable and negligible presence of hydroxyl/epoxy groups (Figure AI. 8 and Table AI. 1). Additionally, the DOS was predicted to contribute more significantly to the kinetics compared to surface modification. Thus for the first time the electrochemical kinetics in the single layer graphene is demonstrated to be highly sensitive to the ADOS upon the addition of even a single H-sp^3 defect per 100,000 sp^2 carbon atoms. More importantly, the correlation between k^o and DOS in return confirms the importance of graphene electronic properties (DOS) in terms of defining the electrochemical current for sensing application.

2.2.9 Correlation between μ and k^o

Figure 2.4e shows the dependence of the relative variation of $\Delta k^o/k^o_{\text{untre}}$ with $\Delta\mu/\mu_{\text{untre}}$, where $\Delta k^o/k^o_{\text{untre}} \frac{\Delta k^o/k^o_{\text{untre}}}{k^o_{\text{untre}}}$, $\Delta\mu/\mu_{\text{untre}} = \frac{\mu-\mu_{\text{untre}}}{\mu_{\text{untre}}}$, and the subscript "untre" denotes untreated graphene. Notably, the negative values of $\Delta\mu/\mu_{\text{untre}}$ corresponds to the degradation of the carrier mobility upon hydrogenation time (see also Figure 2.2). Specifically, the peak value of the $\Delta k^o/k^o_{\text{untre}}$ after one second of hydrogenation is ascribed to the disclosure of the intrinsic electrochemical activity of the graphene basal plane resulting from the volatilization of hydrocarbon adsorbates. For hydrogenation times longer than 3-5 s, $\Delta k^o/k^o_{\text{untre}}$ decreases by ~5 times compared to the peak value (at 1 s) with preserved mobility (~50-60 %). Our results therefore

suggest the importance of H-sp^3 defects towards achieving a low electrochemical activity in GFET by suppressing its DOS. Interestingly, the boosted k^o after surface cleaning reveals a relatively high electrochemical activity of graphene basal plane, which was often believed to be inert and inactive in electrochemistry.[35]

2.3 Discussions

A hydrogen radical plasma is demonstrated to clean the surface of graphene and chemically modify the graphene lattice upon continuous exposure. For the chemical modification, the hydrogen radical forms a covalent bond with the carbon atom in the graphene lattice, changing its hybridization from sp^2 to sp^3. In the beginning (the first 1–5 s), the introduced H radicals mainly sweep the hydrocarbon adsorbates away from the graphene surface. In particular, within the first second of hydrogenation a large enhancement of the electrochemical activity on the surface of pristine graphene (with a minimum of H-sp^3 defects) is observed. It is postulated that in untreated graphene, the electrochemical activity was initially blocked by the presence of hydrocarbon adsorbates which are now removed by the hydrogen plasma[36] (Figure 2.3c and Figure 2.4d). Remarkably, even traces amounts of H-sp^3 defects in graphene (only one sp^3 defect per ~400,000 carbon atoms) results in the decrease of the DOS, a quantity considerably sensitive to the changes of electronic and chemical properties of graphene. Additionally, further hydrogenation of the graphene basal plane largely depresses k^o down to one fifth of its original value (pristine graphene), presumably by lowering its DOS. Interestingly, however, the mobility of graphene is preserved to a large extent (Figure 2.2), promising future development of electrochemical field-effect transistors based on H-graphene.

Given the relatively depressed mobility for the starting samples, the intrinsic defect (i.e. vacancy, grain boundary) and scatterings from the substrate are assumed to already exist. Therefore, the carrier transport properties is limited by the lowest impedance pathways already existing within the graphene lattice. Anything that affects the number of scatters and their cross section will disproportionately register as a mobility change. In other words, it is only specific defects at certain locations that will have the most influence on the mobility. In addition, the mobility changes with the defect density in Figure 2.2d in an implied and non-linear trend. As the density of hydrogenated defect grows, the interdefect distance between defective sites (randomly and uniformly distributed) decreases. In other words, the defect distribution evolves from random to “cluster”. In consequence, the influence of defect at high density level on the transport properties of graphene becomes less sensitive than the low density level.

Besides hydrogenation, the physisorption of water molecules at the graphene surface reflected by the observed p-doping effect (Figure 2.2b)[14] is also considered. As non-covalent functionalization, water molecules can barely disturb the intrinsic aromaticity,[37] and are thus expected to exert little impact on the electronic structure and electrochemistry of graphene[38]. For example, the resistivity at the CNP as well as the carrier mobility barely changed after removal of the adsorbed water[14]. Separately, negligible oxidation is found using XPS characterization even in aged graphene, as shown in Figure AI. 5. Therefore the major contributions of surface-adsorbed water and graphene oxidation can be excluded to the observed electrical and electrochemical properties of hydrogenated graphene.

2.4 Conclusions

In summary, we have systematically probed the interplay between the in-plane electron transport and the electrochemical activity of the graphene basal plane by modulating the density of H-sp^3 defects. Interestingly, the mild hydrogenation within 1–5 s largely preserves the basic electrical mobility while effectively depresses the electrochemical kinetics k^o and lowers the DOS in graphene, manifesting as a plausible way to improve the sensitivity of GFET. For the first time, we demonstrated that the electrochemical kinetics in single layer H-graphene is highly dependent on the ADOS, which supports the theory of non-adiabatic electron transfer on graphene. Additionally, the electrochemical activity of the pristine graphene basal plane can be restored by the removal of surface-adsorbed hydrocarbons using a low dose of hydrogen radicals, a result that will further promote graphene as an electrode for electrochemical studies. The correlation between the carrier mobility and the electrochemical kinetics suggests that the electrical conductivity of H-graphene is an important parameter to consider, for example, in GEC sensors. We believe our work will inspire several research communities to consider hydrogenated graphene as a potent material for sensing applications with performances going beyond previously reported (G)FET sensors.

2.5 References

[1] a) A. Zhang, C. M. Lieber, *Chem. Rev.* **2015**, 116, 215; b) W. Fu, L. Jiang, E. P. van Geest, L. Lima, G. F. Schneider, *Adv. Mater.* **2016**, 6, 1603610.

[2] a) M. T. Hwang, P. B. Landon, J. Lee, D. Choi, A. H. Mo, G. Glinsky, R. Lal, *Proc. Natl. Acad. Sci.* **2016**, 113, 7088; b) N. Gao, T. Gao, X. Yang, X. Dai, W. Zhou, A. Zhang, C. M. Lieber, *Proc. Natl. Acad. Sci.* **2016**, 113, 14633.

[3] a) Y. Wang, Y. Shao, D. W. Matson, J. Li, Y. Lin, *ACS nano* **2010**, 4, 1790; b) Z. Xia, F. Leonardi, M. Gobbi, Y. Liu, V. Bellani, A. Liscio, A. Kovtun, R. Li, X. Feng, E. Orgiu, *ACS Nano* **2016**, 10, 7125; c) P. Fortgang, T. Tite, V. Barnier, N. Zehani, C. Maddi, F. Lagarde, A.-S. Loir, N. Jaffrezic-Renault, C. Donnet, F. Garrelie, *ACS Appl. Mater. Interfaces* **2016**, 8, 1424; d) A. Y. S. Eng, Z. Sofer, Š. Huber, D. Bouša, M. Maryško, M. Pumera, *Chem. Eur. J.* **2015**, 21, 16828.

[4] a) S. Eigler, A. Hirsch, *Angew. Chem. Int. Ed.* **2014**, 53, 7720; b) Z. Bai, L. Zhang, L. Liu, *J. Phys. Chem. C* **2015**, 119, 26793; c) A. Bagri, C. Mattevi, M. Acik, Y. J. Chabal, M. Chhowalla, V. B. Shenoy, *Nat. Chem.* **2010**, 2, 581.

[5] a) Z. Sun, C. L. Pint, D. C. Marcano, C. Zhang, J. Yao, G. Ruan, Z. Yan, Y. Zhu, R. H. Hauge, J. M. Tour, *Nat. Commun.* **2011**, 2, 559; b) D. C. Elias, R. R. Nair, T. Mohiuddin, S. Morozov, P. Blake, M. Halsall, A. Ferrari, D. Boukhvalov, M. Katsnelson, A. Geim, *Science* **2009**, 323, 610; c) R. R. Nair, W. Ren, R. Jalil, I. Riaz, V. G. Kravets, L. Britnell, P. Blake, F. Schedin, A. S. Mayorov, S. Yuan, *Small* **2010**, 6, 2877; d) J. Son, S. Lee, S. J. Kim, B. C. Park, H.-K. Lee, S. Kim, J. H. Kim, B. H. Hong, J. Hong, *Nat. Commun.* **2016**, 7, 13261.

[6] F. Tuinstra, J. L. Koenig, *J. Chem. Phys.* **1970**, 53, 1126.

[7] P. Lespade, A. Marchand, M. Couzi, F. Cruege, *Carbon* **1984**, 22, 375.

[8] A. Eckmann, A. Felten, A. Mishchenko, L. Britnell, R. Krupke, K. S. Novoselov, C. Casiraghi, *Nano Lett.* **2012**, 12, 3925.

[9] a) A. Das, S. Pisana, B. Chakraborty, S. Piscanec, S. Saha, U. Waghmare, K. Novoselov, H. Krishnamurthy, A. Geim, A. Ferrari, *Nat. Nanotechnol.* **2008**, 3, 210; b) Q. H. Wang, C.-J. Shih, G. L. Paulus, M. S. Strano, *J. Am. Chem. Soc.* **2013**, 135, 18866.

[10] L. G. Cançado, A. Jorio, E. M. Ferreira, F. Stavale, C. Achete, R. Capaz, M. Moutinho, A. Lombardo, T. Kulmala, A. Ferrari, *Nano Lett.* **2011**, 11, 3190.

[11] A. C. Ferrari, D. M. Basko, *Nat. Nanotechnol.* **2013**, 8, 235.

[12] W. Fu, C. Nef, A. Tarasov, M. Wipf, R. Stoop, O. Knopfmacher, M. Weiss, M. Calame, C. Schönenberger, *Nanoscale* **2013**, 5, 12104.

[13] N. B. Cramer, C. L. Couch, K. M. Schreck, J. A. Carioscia, J. E. Boulden, J. W. Stansbury, C. N. Bowman, *Dent. Mater.* **2010**, 26, 21.

[14] B. R. Matis, J. S. Burgess, F. A. Bulat, A. L. Friedman, B. H. Houston, J. W. Baldwin, *ACS Nano* **2012**, 6, 17.

[15] a) F. Schedin, A. Geim, S. Morozov, E. Hill, P. Blake, M. Katsnelson, K. Novoselov, *Nature materials* **2007**, 6, 652; b) E. Hwang, S. Adam, S. D. Sarma, *Phys. Rev. Lett.* **2007**, 98, 186806; c) M. Trushin, J. Schliemann, *EPL (Europhysics Letters)* **2008**, 83, 17001.

[16] J. Balakrishnan, G. K. W. Koon, M. Jaiswal, A. C. Neto, B. Özyilmaz, *Nat. Phys.* **2013**, 9, 284.

[17] I. Heller, J. Kong, K. A. Williams, C. Dekker, S. G. Lemay, *J. Am. Chem. Soc.* **2006**, 128, 7353.

[18] J. Xia, F. Chen, J. Li, N. Tao, *Nat. Nanotechnol.* **2009**, 4, 505.

[19] M. Velicky, D. F. Bradley, A. J. Cooper, E. W. Hill, I. A. Kinloch, A. Mishchenko, K. S. Novoselov, H. V. Patten, P. S. Toth, A. T. Valota, *ACS Nano* **2014**, 8, 10089.

[20] R. S. Nicholson, *Anal. Chem.* **1965**, 37, 1351.

[21] H. Ji, X. Zhao, Z. Qiao, J. Jung, Y. Zhu, Y. Lu, L. L. Zhang, A. H. MacDonald, R. S. Ruoff, *Nat. Commun.* **2014**, 5, 3317.

[22] J.-H. Zhong, J. Zhang, X. Jin, J.-Y. Liu, Q. Li, M.-H. Li, W. Cai, D.-Y. Wu, D. Zhan, B. Ren, *J. Am. Chem. Soc.* **2014**, 136, 16609.

[23] A. Eckmann, A. Felten, I. Verzhbitskiy, R. Davey, C. Casiraghi, *Phys. Rev. B* **2013**, 88, 035426.

[24] Z. Li, Y. Wang, A. Kozbial, G. Shenoy, F. Zhou, R. McGinley, P. Ireland, B. Morganstein, A. Kunkel, S. P. Surwade, L. Li, H. Liu, *Nat. Mater.* **2013**, 12, 925.

[25] a) A. N. Patel, M. G. Collignon, M. A. O'Connell, W. O. Y. Hung, K. McKelvey, J. V. Macpherson, P. R. Unwin, *J. Am. Chem. Soc.* **2012**, 134, 20117; b) M. Velický, M. A. Bissett, P. S. Toth, H. V. Patten, S. D. Worrall, A. N. J. Rodgers, E. W. Hill, I. A. Kinloch, K. S. Novoselov, T. Georgiou, L. Britnell, R. A. W. Dryfe, *Phys. Chem. Chem. Phys.* **2015**, 17, 17844.

[26] Y.-D. Lim, D.-Y. Lee, T.-Z. Shen, C.-H. Ra, J.-Y. Choi, W. J. Yoo, *ACS Nano* **2012**, 6, 4410.

[27] J.-H. Chen, C. Jang, S. Adam, M. Fuhrer, E. Williams, M. Ishigami, *Nat. Phys.* **2008**, 4, 377.

[28] S. Adam, E. Hwang, E. Rossi, S. D. Sarma, *Solid State Commun.* **2009**, 149, 1072.

[29] G. L. Paulus, Q. H. Wang, M. S. Strano, *Acc. Chem. Res.* **2012**, 46, 160.

[30] D. M. Adams, L. Brus, C. E. Chidsey, S. Creager, C. Creutz, C. R. Kagan, P. V. Kamat, M. Lieberman, S. Lindsay, R. A. Marcus, *J. Phys. Chem. B* **2003**, 107, 6668.

[31] J. Eisenstein, L. Pfeiffer, K. West, *Phys. Rev. Lett.* **1992**, 68, 674.

[32] V. Levich, *Physical chemistry, and advanced treatise, vol Xb. Academic, New York* **1970**.

[33] R. Nissim, C. Batchelor-McAuley, M. C. Henstridge, R. G. Compton, *Chem. Commun.* **2012**, 48, 3294.

[34] A. M. Debela, M. Ortiz, V. Beni, C. K. O'Sullivan, *Chem. Eur. J.* **2014**, 20, 7646.

[35] D. A. C. Brownson, D. K. Kampouris, C. E. Banks, *Chem. Soc. Rev.* **2012**, 41, 6944.

[36] Z. Li, A. Kozbial, N. Nioradze, D. Parobek, G. J. Shenoy, M. Salim, S. Amemiya, L. Li, H. Liu, *ACS Nano* **2016**, 10, 349.

[37] Z. Zhang, H. Huang, X. Yang, L. Zang, *J. Phys. Chem. Lett.* **2011**, 2, 2897.

[38] Y. F. Peng, J. Wang, Z. S. Lu, X. Y. Han, *IOP Conf. Ser. Mater. Sci. Eng.* **2015**, 87, 012101.